The Cryosphere Discuss., 2, 225–254, 2008
www.the-cryosphere-discuss.net/2/225/2008/

The Cryosphere Discussions

The Cryosphere Discussions is the access reviewed discussion forum of *The Cryosphere*

Estimation of the Greenland ice sheet surface mass balance during 20th and 21st centuries

X. Fettweis[1], E. Hanna[2], H. Gallée[3], P. Huybrechts[4], and M. Erpicum[1]

[1]Département de Géographie, Université de Liège, Belgium
[2]Department of Geography, University of Sheffield, UK
[3]LGGE – Laboratoire de Glaciologie et Géophysique de l'Environnement, Grenoble, France
[4]Departement Geografie, Vrije Universiteit Brussel, Belgium

Received: 6 March 2008 – Accepted: 17 March 2008 – Published: 9 April 2008

Correspondence to: X. Fettweis (xavier.fettweis@ulg.ac.be)

Published by Copernicus Publications on behalf of the European Geosciences Union.

Abstract

Results from a regional climate simulation (1970–2006) over the Greenland ice sheet (GrIS) reveals that more than 97% of the interannual variability of the modelled Surface Mass Balance (SMB) can be explained by the GrIS summer temperature anomaly and the GrIS annual precipitation anomaly. This multiple regression is then used to empirically estimate the GrIS SMB since 1900 from climatological time series. The projected SMB changes in the 21st century are investigated with the set of simulations performed with atmosphere-ocean general circulation models (AOGCMs) of the Fourth Assessment Report of the Intergovernmental Panel on Climate Change (IPCC AR4). These estimates show that the high surface mass loss rates of recent years are not unprecedented in the GrIS history of the last hundred years. The minimum SMB rate seems to have occurred earlier in the 1930s. The AOGCMs project that the SMB rate of the 1930s would be common at the end of 2100. The temperature would be higher than in the 1930s but the increase of accumulation in the 21st century would partly offset the acceleration of surface melt due to the temperature increase. However, these assumptions are based on an empirical multiple regression only validated for recent/current climatic conditions, and the accuracy and time homogeneity of the data sets and AOGCM results used in these estimations constitute a large uncertainty.

1 Introduction

Mass balance variations of the GrIS play an important role in global sea level fluctuations and oceanic THC changes. On the one hand, GrIS mass balance changes appear to have contributed several metres to some of the sea-level fluctuations since the last interglacial period known as the Eemian, 1.25×10^5 yr ago (Cuffey and Marshall, 2000) and are expected to contribute to sea-level rise under the projected future global warming throughout this century (IPCC, 2007). On the other hand, increases in the freshwater flux from the Greenland ice sheet (run-off of the surface melt water, basal melting

TCD
2, 225–254, 2008

and glacier discharge) could perturb the THC by reducing the density contrast driving the thermohaline circulation (Rahmstorf et al., 2005). Any weakening of the THC in response to a surface warming and an increasing freshwater flux induced by global warming (Gregory et al., 2005; Swingedouw et al., 2006) would reduce the heat input to the North Atlantic ocean and subsequently reduce the warming in regions including Europe. The IPCC 4th Assessment Report (IPCC AR4) projects that the Greenland ice sheet is likely to lose mass because the increasing run-off is expected to exceed the precipitation increase in a warmer climate but did not expand on the individual model estimates or mass balance components.

In this study, we provide estimates of the GrIS SMB from 1900 to 2100 based on a multiple regression model using anomalies of GrIS summer temperature (from 1 June to 31 August) and from GrIS annual precipitation. A 37-yr (1970–2006) simulation of the GrIS performed by the regional climate model MAR (Modèle Atmosphérique Régional) shows that 97% of the interannual variability of the modelled SMB is explained by these anomalies (Fettweis, 2007). Such a strong correlation is also confirmed by the model of Hanna et al. (2008) driven by the ECMWF (re)analysis. We use this relation to empirically estimate the GrIS SMB since 1900 until now from climatological time series and analyses. The 21st century is investigated with results from the AOGCMs used in the IPCC AR4. Sect. 2 explains in detail both the method and data used. Estimates of near past and future GrIS SMB rates are presented in Sect. 3 and Sect. 4, respectively. Section 5 contains a discussion of the results.

2 Method

To a first approximation, the GrIS SMB variability (ΔSMB_{GrIS}) is driven by the GrIS annual precipitation anomaly (ΔP_{yr}) minus the GrIS meltwater run-off rate variability. According to Box et al. (2004) and Fettweis (2007), the run-off rate variability can be approximated by the GrIS summer (from 1 June to 31 August) 3 m-temperature (ΔT_{jja})

to give this multiple regression:

$$\Delta SMB_{GrIS} \simeq a\Delta T_{jja} + b\Delta P_{yr} \quad (1)$$

where a and b are constant parameters. These parameters are determined by resolving the multiple regression equation using the simulated GrIS SMB anomaly time series and both temperature and precipitation anomaly time series.

By using de-trended results simulated by MAR, a correlation coefficient of 0.97 is obtained between the simulated and estimated GrIS SMB anomaly from Eq. (1) over the period 1970–1999. The root mean square error (RMSE) represents 25% of the GrIS SMB anomaly standard deviation. Such a correlation motivated the use of this equation to extend the estimate of the SMB variability with the help of climatological time series and the outputs from analyses and the AOGCMs used in the IPCC AR4. The 30-yr reference period (1970–1999) is chosen because it covers most of the available data sets and model results used in this study.

Figure 1 shows where the regional variability of the MAR 3 m-temperature and precipitation best captures the variability of the MAR SMB of the whole ice sheet. With the aim of applying this multiple regression to other data sets (at low resolution and without an ice sheet/land mask), we delimited regions in latitude/longitude on the GrIS where the variability of precipitation and temperature will be captured to estimate the SMB following Eq. (1). These regions (called Region 1 and Region 2 hereafter) are different for temperature and precipitation, and are plotted in Figs. 1 and 2. The boundaries of these regions are chosen to have higher correlations between the GrIS SMB modelled by MAR and the SMB estimated by temperature/precipitation anomaly simulated by MAR model (following Fig. 1) as well as anomalies from all data sets used hereafter (see Table 2). Both regions chosen are therefore the same for all data sets.

The excellent agreement between the modelling from MAR and from Hanna et al. (2008) (called Hanna08 hereafter) and the estimates of the GrIS SMB anomaly by using temperature (resp. precipitation) anomaly on Region 1 (resp. 2) can be seen in Fig. 3. This figure compares also the GrIS SMB simulated by the Polar MM5 model

(Box et al., 2006). The interannual variability between the three models compares very well. In the 2000s, the MAR SMB anomalies are much lower than the other models and the agreement between simulated and estimated SMB (from Eq. 1) is worse. The results are likely affected in part by inhomogeneities after 2002 due to the use of the operational ECMWF analysis, instead of the model-consistent ECMWF reanalysis for the period 1958–2001, to drive the three models. The disagreement in the 2000s explains why we did not extend the 30-yr reference period (1970–1999) to the 2000s.

3 Surface mass balance in the 20th century

For each data set listed in Table 1, we computed the parameters a and b over the reference period (1970–1999) by using the GrIS SMB anomaly time series simulated by MAR and by Hanna08 in the left part of Eq. (1) and the temperature/precipitation anomaly time series from the data set averaged on Region 1/Region 2 in the right part. The high correlation coefficient(>0.8) between the GrIS SMB anomaly simulated by MAR (resp. Hanna08) and the one estimated by the data sets following Eq. (1) over 1970–1999 (see Tables 2 and 3) motivated us to extend empirically the SMB anomaly estimation to the whole period covered by the data sets by using the same previously determined parameters a and b. These parameters are computed over 1970–1999 by using de-trended (i.e. with a zero trend) time series to minimise the dependence on the reference period and are applied after that to the whole time series (without correction of the trend). The anomalies refer then to the period 1970–1999. In addition, the use of de-trended time series of anomalies to compute the parameters a and b rather than time series of values provides a better homogeneity between the different data sets and the MAR (resp. Hanna08) model.

Before continuing, it should be noted that these data set-based SMB anomaly estimates should be considered with precaution.

– Firstly, these estimates are based on Eq. (1) which does not explain fully the

SMB variability and uses results from the MAR and Hanna08 models (not direct observations) for the calibration.

- Secondly, by using constant parameters *a* and *b* through the whole period covered by the climatic dataset, we assume that the dependence of the SMB on the temperature/precipitation anomaly are the same as during 1970–1999. That is why we chose to use de-trended time series to minimise this impact.
- In addition, we assume that the data set is homogeneous through the whole period, which is not guaranteed as, for example, in the ECMWF time series after 2002.
- We assume also that the variability in Region 1 and 2 remains representative for the whole ice sheet for the entire period.
- Finally, there are not many in-situ observations (on which the data sets are based) available over Greenland. Such data are collected along the coast by the Danish Meteorological Institute (DMI) weather stations. They are consequently not representative for the GrIS (Fettweis et al., 2005; Cappelen et al., 2001), although Hanna et al. (2008) show good correspondence between DMI and Swiss Camp (west flank of GrIS) summer temperature variations since 1990. Nevertheless, we can assume that the interannual variability is less sensitive to the lack of measurements over the GrIS, the more so since the variability along the coast is a good proxy for the whole GrIS variability according to Figs. 1 and 2.

Figure 4 plots the time series of anomalies for the different datasets from 1900 to 2006. As these datasets are mainly based on the same in situ observations, the temperature time series compare very well. All the series unanimously show warm periods around 1930, 1950 and 1960 in full agreement with previous studies based on coastal DMI weather station observations (Box, 2002; Box and Cohen, 2006; Vinther et al., 2006). The rate of warming in 1920–1930 is the most spectacular as pointed out by Chylek et al. (2006). Finally, Greenland climate was colder around 1920 and, in the

1970s and 1980s. The temperature minimum (resp. maximum) seems to have occurred in 1992 after the Mont Pinatubo eruption (resp. in 1931). The warm summers of recent years (1998, 2003, 2005), associated with large melt extent areas (Fettweis et al., 2007), seem to be less warm than these of the 1930s, as also pointed out by Hanna et al. (2007).

Concerning the precipitation time series, the agreement among them is less obvious and large disparities occur as for example with the NCEP precipitation time series in the 1950s. In addition, the interannual variability is more significant in the GHCN precipitation time series because only one or two pixels with data are available in Region 2 (Three pixels with temperature data are available in Region 1). This suggests that the precipitation variability in the GHCN time series is rather the variability measured by one or two coastal DMI weather stations. However, the series show all a small negative anomaly in the 1930s and positive in 1970s but these anomalies are less significant than the temperature anomalies. Finally, the correlation of the de-trended time series of the data sets with the MAR anomalies is better for temperature than for precipitation (see Table 2). The precipitation is more difficult to simulate and to measure (especially snowfall) which might explain these discrepancies.

Both simulated and estimated SMB anomalies through the 20th century are plotted on Fig. 5. The reference period is 1970–1999 over which the GrIS SMB simulated by MAR is $352 \pm 112\,\mathrm{km^3\,yr^{-1}}$ (resp. $348 \pm 105\,\mathrm{km^3\,yr^{-1}}$ for Hanna08). The generally accepted current estimate of the GrIS SMB is around $300\,\mathrm{km^3\,yr^{-1}}$ which approximately balances the glacier discharge and the basal melting rate (Reeh et al., 1999; Fettweis, 2007). Tables 2 and 3 list the ratio a/b, i.e. the weight of the temperature variability against the precipitation variability in the SMB variability. This ratio is obtained by using normalised (i.e. varying between -1 and $+1$) de-trended temperature/precipitation anomaly time series. On average, this ratio is near -1.5 (resp. -1) if the SMB anomaly time series simulated by MAR (resp. Hanna08) is used to calibrate a and b. Therefore, thermal factors, rather than precipitation changes, influence the SMB sensitivity, as concluded by Fettweis (2007). This ratio is above -1 with the GHCN time series

but these data should be considered with caution due to the sparse data available in Region 1 and 2.

The set of SMB estimates in Fig. 5 agree to give positive anomalies around 1920 and in the 1970s and 1980s. The maximum, confirmed by all data sets, takes place at the beginning of the 1970s with a SMB anomaly near $+200\,km^3\,yr^{-1}$ due to a combination of cold summers and wet years. Over the period 1930–1960 and since the end of 1990s, the estimated SMB is below the 1970–1999 average. The absolute minimum occurred around 1930 with a SMB anomaly near $-300\,km^3\,yr^{-1}$. Secondary (minor) SMB minima appear to have occurred in 1950 and 1960, equalling the surface mass loss rates of the last few years (1998, 2003, 2006), although these minima are not confirmed in all data sets. However (Chylek et al., 2007) found also a maximum melt area at the beginning of the 1930s followed by minor maxima in 1950 and 1960. The minimum SMB rates around 1930 are due to exceptionally warm summers combined with dry years inducing SMB rates lower than those currently observed, although the effect of human-induced global warming was not perceptible at that time. Around 1950 and 1960, the low SMB rates are mainly explained by positive temperature anomalies. This suggests that the glacier acceleration observed in the last decade (Rignot and Kanagaratnam, 2006) is likely to have occurred previously as well in the 1930s if the melt-induced outlet glacier acceleration is confirmed (Zwally et al., 2002). Therefore, the whole ice-sheet mass balance was likely to have been negative at that time. After the 1990s, the GrIS SMB decreases slowly to reach the negative anomalies of the last few years, although the summers of the 2000s were not exceptional compared to 70 yr ago (Chylek et al., 2006).

Finally, the interannual SMB variability was higher in 1960–1990 than in the 1930s and 2000s. During 1960–1990, negative SMB anomalies were mainly succeeded by positive anomalies. By contrast, in the 1930s and 2000s, there is a succession of negative SMB anomalies inducing an acceleration of the melt due to the albedo feedback. A high melt-rate year decreases the snow pack albedo for the next year if the winter accumulation is not enough to compensate the melt during the next summer (Fettweis,

2007).

4 Change in the future

In the following section, we assume that the hypotheses made before are still valid in the near future. In that case, AOGCM simulations performed for the IPCC AR4 can be used to project the GrIS SMB anomalies for the 21st century. The projected temperature/precipitation anomalies (plotted in Fig. 6) are based on model outputs from the "Climate of the Twentieth Century Experiment" (20C3M) and from the scenario SRES (Special Report on Emission Scenarios) A1B described in Nakicenov and Swart (2000). The mid-range A1B scenario corresponds to a continuous increase of the atmospheric CO_2 concentration during the 21st century to a level of 720 ppm by 2100.

We deduce the projected SMB changes in the future from the IPCC AR4 experiments via the following algorithm:

1. The time series of temperature (ΔT_i) and precipitation (ΔP_i) from the 20C3M experiment are de-trended, centred i.e.

$$\overline{\Delta T} = \frac{1}{30} \sum_{i=1970}^{1999} \Delta T_i = \overline{\Delta P} = 0 \quad (2)$$

and normalised i.e.

$$\Delta T_i \text{ and } \Delta P_i \in [-1, 1] \quad (3)$$

over 1970–1999. The normalisation of the ΔT_i and ΔP_i time series enables to homogenise the AOGCMs results over 1970–1999.

2. The MAR and Hanna08 results show a standard deviation of the GrIS SMB time series around 100 $km^3\,yr^{-1}$ over the period 1970–1999. Therefore, if $k=a/b$, the

standard deviation of the SMB estimated by the temperature and precipitation time series from the 20C3M experiment is fixed to be 100 $km^3\,yr^{-1}$, i.e.

$$\sqrt{\sum_{i=1970}^{1999} (a(\Delta T_i - \overline{\Delta T}) + b(\Delta P_i - \overline{\Delta P}))^2} \quad (4)$$

$$= a\sqrt{\sum_{i=1970}^{1999} (\Delta T_i + 1/k\,\Delta P_i)^2} \quad (5)$$

$$= 100\ km^3\ yr^{-1} \quad (6)$$

which enables the computation of a and b if the parameter k is known. Previous results listed in Tables 2 and 3 show a parameter k varying between −1.8 and −0.6 following the data and model results used. Here, we will compute a and b for k fixed at both −2 and −1.

3. For each decade between the 2010s and the 2090s, the mean projected temperature (resp. precipitation) in Region 1 (resp. Region 2) is retrieved from the SRESA1B scenario. Afterwards, the mean 1970–1999 temperature (resp. precipitation) from the 20C3M experiment is subtracted from the projected temperature (resp. precipitation) to compute anomalies which we divide by the normalisation factor used in Eq. (3). By using parameters a and b computed in Eq. (4), we can then estimate the projected SMB anomaly for each decade based on a fixed value of k.

As validation, this algorithm was applied to the ECMWF (resp. GHCN) time series by taking a value of −1 for the parameter k. The resulted estimated SMB time series fully agree with these simulated by Hanna08. The correlation coefficient is 0.97 (resp. 0.85) for a RMSE equal to 32 (resp. 52) $km^3\,yr^{-1}$. These results should be compared with those listed in Table 3.

Figure 6 plots the decadal mean of the temperature and precipitation anomalies for all models listed in Table 4. While the interdecadal variability is very high (particularly for precipitation) and some models are in total disagreement with the others, the models are unanimous in projecting a temperature increase of ~2.5°C through the 21st century. Changes in precipitation are more model-dependent than temperature although the multimodel average gives a small increase of precipitation during the 21st century. Table 5 summarises the changes projected for the 21st century.

The ensemble mean of the 23 models used in the 20C3M experiment (see Table 4) gives a mean surface temperature (resp. precipitation) of -1.2 ± 0.6°C (resp. 530 ± 60 mm) and a trend of $+0.02\,\mathrm{K^{\circ}\,yr^{-1}}$ (resp. no significant precipitation change) in Region 1 (resp. Region 2) over the reference period 1979–1999. These results are in agreement with observations during 1970-1999, suggesting that the multimodel average can be used as a reliable estimate of future changes. In a first approach, we decided to use only results of the ensemble mean rather than those from a single model. Sophisticated weighting of the various models can be investigated in the future.

The SMB anomaly projection for $k=a/b=-1$ and $k=-2$ are shown in Fig. 7 and listed in Table 5. The lower SMB anomaly in the 20th century seems to have occurred in 1931 with $-300\,\mathrm{km^3\,yr^{-1}}$. This record surface mass loss rate is likely to become common at the end of the 21st century. The temperature will probably be much higher than previously observed during the 20th century, but a predicted increase of precipitation will most likely partly offset the SMB decrease associated with warming. With the SRESA2 experiment, the projected negative SMB anomaly is higher. However it should be noted that the MAR model simulates for 2003 and 2006 negative SMB anomalies equivalent to those projected by the AOGCMs on average for the end of the 21st century. These recent SMB rates are the result of low precipitation and very high temperatures (an anomaly of about 2 °K occurred in 2003), suggesting that some AOGCMs could underestimate changes resulting from the global warming over the GrIS.

These projections are decadal means suggesting that some SMB anomalies could

be much lower for individual years (see Fig. 8) owing to the high observed interannual variability in the SMB (see Fig. 3). In addition to the uncertainties linked to the models/scenario and the value of k, these projections do not take into account changes in ice dynamics and surface topography as described in Gregory and Huybrechts (2006). An albedo decrease as well as a decrease of the surface height due to successive annual negative GrIS mass rates induces an acceleration of the melt. In addition to these surface changes, there may be changes in glacier discharge (e.g. from melt-induced outlet glacier acceleration as observed by Zwally et al., 2002) and in basal melting estimated currently to be $\sim 300\,km^3\,yr^{-1}$ by Reeh et al. (1999).

If we assume that the whole GrIS was in balance in 1970–1999, the mass loss from glacier discharge and basal melting to equilibrate the simulated SMB is $+350\,km^3\,yr^{-1}$. At the end of this century, the mean projections estimate SMB anomalies reaching as low as about $-300\,km^3\,yr^{-1}$ which gives a global average rate of sea level rise of $+0.83\,mm\,yr^{-1}$ (the computation was made by using an area of a world ocean area of 361 million km^2). These rates are entirely in agreement with those published by Huybrechts et al. (2004) and by Gregory and Huybrechts (2006) for a similar scenario. The mean SMB could be $+50\,km^3\,yr^{-1}$ in 2100. Added to the current mass loss from glacier discharge and basal melting ($\sim -350\,km^3\,yr^{-1}$), the whole GrIS mass balance would be $-300\,km^3\,yr^{-1}$. The total volume of the GrIS is $2.93\times10^6\,km^3$ according to Bamber et al. (2001). About ten thousand years would be needed to melt the ice sheet completely with a constant rate of $-300\,km^3\,yr^{-1}$. This simple calculation does not take into account the positive feedbacks from albedo and elevation changes (Ridley et al., 2005) or changes in ice dynamics nor the fact that in a warmer climate the ice sheet will retreat from the coast so that less calving can take place.

5 Discussion and conclusion

Simulations made with MAR (Fettweis, 2007) and by Hanna et al. (2008) reveal a very high correlation between the interannual variability of the modelled SMB and the

variability of both temperature and precipitation GrIS anomalies. We have derived a multiple-regression relation that has been used with climatological time series to empirically estimate the GrIS SMB since 1900. The SMB changes projected for the end of the 21st century have been derived using the set of experiments conducted for the IPCC AR4.

The results show that the GrIS surface mass loss in the 1930s is likely to have been more significant than currently due to a combination of very warm and dry years. It is also noted from our results that a mere ten years would be enough to pass from a GrIS growth state to a significant mass-loss state. Therefore, the SMB changes that are currently occurring, and which are linked to global warming (Fettweis, 2007; Hanna et al., 2008) are not exceptional in the GrIS history. For the near future, the IPCC AR4 models project SMB rates similar to those of the 1930s for the end of the 21st century. That transforms to about 4 cm of sea-level rise for the end of this century under SRES scenario A1B. If these rates are confirmed and no significant changes occur in iceberg calving and basal melting, then these rates are not large enough to significantly change the freshwater flux into the Atlantic Ocean. However, large uncertainties remain indeed in these estimates due to models/scenarios used as well as parameters and hypotheses made in the algorithm to estimate the GrIS SMB anomaly. That is why further investigations are needed. High-resolution simulations made with the MAR model (which explicitly simulates the SMB by incorporating the surface feedbacks) forced at its boundaries by the IPCC AR4 models outputs should yield more comprehensive and realistic results although this requires a lot of computing time. Moreover, both 2003 and 2006 negative SMB anomalies simulated by MAR resulting from a combination of low precipitation and very high temperatures are equivalent to those projected by the AOGCMs on average for the end of the 21st century. This suggests that some AOGCMs could underestimate changes over the GrIS from the global warming.

Acknowledgements. We acknowledge the modelling groups, the Program for Climate Model Diagnosis and Intercomparison (PCMDI) and the WCRP's Working Group on Coupled Modelling (WGCM) for their roles in making available the WCRP CMIP3 multi-model dataset. Support of this dataset is provided by the Office of Science, US Department of Energy.

References

Bamber, J. L., Layberry, R. L., and Gogineni, S. P.: A new ice thickness and bed data set for the Greenland ice sheet: part I, Measurement, data reduction, and errors, J. Geophys. Res., 106, 33 773–33 780, 2001. 236

Box, J. E.: Survey of Greenland instrumental temperature records: 1873–2001, Int. J. Climatol., 22, 1829–1847, 2002. 230

Box, J. E., Bromwich, D. H., and Bai, L.-S.:Greenland ice sheet surface mass balance for 1991–2000: application of Polar MM5 mesoscale model and in-situ data, J. Geophys. Res., 109(D16), D16105, doi:10.1029/2003JD004451, 2004. 227

Box, J. E. and Cohen, A. E.:Upper-air temperatures around Greenland: 1964–2005, Geophys. Res. Lett., 33, L12706, doi:10.1029/2006GL025723, 2006. 230

Box, J. E., Bromwich, D. H., Veenhuis, B. A., Bai, L.-S., Stroeve, J. C., Rogers, J. C., Steffen, K., Haran, T., and Wang, S.-H.: Greenland ice sheet surface mass balance variability (1988–2004) from calibrated Polar MM5 output, J. Climate, 19(12), 2783–2800, 2006. 229, 249

Cappelen, J., Jorgensen, B. V., Laursen, E. V., Stannius, L. S., and Thomsen, R. S.: The observed climate of Greenland, 1958–99 – with climatological standard normals, 1961–1990. Tech. Rep. 00-18, 152 pp., Danish Meteorological Institute, Copenhagen, 2001. 230

Chylek, P., Dubey, M. K., and Lesins, G.: Greenland warming of 1920–1930 and 1995–2005, Geophys. Res. Lett., 33, L11707, doi:10.1029/2006GL026510, 2006. 230, 232

Chylek, P., McCabe, M., Dubey, M. K., and Dozier, J.: Remote sensing of Greenland ice sheet using multispectral near-infrared and visible radiances, J. Geophys. Res., 112, D24S20, doi:10.1029/2007JD008742, 2007. 232

Christy, J. R., Spencer, R. W., and Braswell, W. D.: MSU Tropospheric temperatures: Data set construction and radiosonde comparisons, J. Atmos. Ocean. Tech., 17, 1153–1170, 2000.

Cuffey, K. M. and Marshall, S. J.: Substantial contribution to sea level rise during the last interglacial from the Greenland ice sheet, Nature, 404, 591–594, 2000. 226

Dai, A., Fung, I. Y., and Del Genio, A. D.: Surface observed global land precipitation variations during 1900–1988, J. Climate, 10, 2943–2962, 1997.

Fettweis, X., Gallée, H., Lefebre, L., and van Ypersele, J.-P.: Greenland surface mass balance simulated by a regional climate model and comparison with satellite derived data in 1990–1991, Clim. Dynam., 24, 623–640, doi:10.1007/s00382-005-0010-y, 2005. 230

Fettweis, X., van Ypersele, J.-P., Gallée, H., Lefebre, F., and Lefebvre, W.: The 1979–2005 Greenland ice sheet melt extent from passive microwave data using an improved version of the melt retrieval XPGR algorithm, Geophys. Res. Lett., 34, L05502, doi:10.1029/2006GL028787, 2007. 231

Fettweis, X.: Reconstruction of the 1979–2006 Greenland ice sheet surface mass balance using the regional climate model MAR, The Cryosphere, 1, 21–40, 2007. 227, 231, 232, 236, 237

Gregory, J., Dixon, K., Stouffer, R. J., Weaver, A., Driesschaert, E., Eby, M., Fichefet, T., Hasumi, H., Hu, A., Jungclaus, J., Kamenkovich, I., Levermann, A., Montoya, M., Murakami, S., Nawrath, S., Oka, A., Sokolov, A., and Thorpe, R.: A model intercomparison of changes in the Atlantic thermohaline circulation in response to increasing atmospheric concentration, Geophys. Res. Lett.,32, L12703, doi:10.1029/2005GL023209, 2005. 227

Gregory, J. and Huybrechts, P.: Ice-sheet contributions to future sea-level change, Philos. T. R. Soc. A, 364, 1709–1731, 2006. 236

Hanna, E., Box, J., and Huybrechts, P.: Greenland Ice Sheet mass balance, Arctic Report Card 2007, update to State of Arctic Report 2006, NOAA, available at http://www.arctic.noaa.gov/reportcard/, 2007. 231

Hanna, E., Huybrechts, P., Steffen, K. , Cappelen, J., Huff, R., Shuman, C., Irvine-Fynn, T., Wise, S., and Griffiths, M.: Increased runoff from melt from the Greenland Ice Sheet: a response to global warming, J. Climate, 21, 331–341, 2008. 227, 228, 230, 236, 237, 249

Huybrechts, P., Gregory, J., Janssens, I., and Wild, M.: Modelling Antarctic and Greenland volume changes during the 20th and 21st centuries forced by GCM time slice integrations, Global Planet. Change, 42, 83–105, doi:10.1016/j.gloplacha.2003.11.011, 2004. 236

Kalnay, E., Kanamitsu, M., Kistler, R., Collins, W., Deaven, D., Gandin, L., Iredell, M., Saha, S., White, G., Woollen, J., Zhu, Y., Leetmaa, A., Reynolds, B., Chelliah, M., Ebisuzaki, W., Higgins, W., Janowiak, J., Mo, K., Ropelewski, C., Wang, J., Jenne, R., and Joseph, D.: The NCEP/NCAR 40-Year Reanalysis Project, B. Am. Meteorol. Soc., 77, 437–471, 1996. 242

Mitchell, T. D. and Jones, P. D.: An improved method of constructing a database of monthly

climate observations and associated high-resolution grids, Int. J. Climatol., 25, 693–712, 2005. 242
Nakicenov, N. and Swart, R.: Special report on emissions scenarios, Cambridge University Press, Cambridge, 599 pp., 2000. 233
Peterson, T. C. and Vose, R. S.: An overview of the Global Historical Climatology Network temperature database, B. Am. Meteorol. Soc., 78(12), 2837–2849, 1997. 242
Rahmstorf, S., Crucifix, M., Ganopolski, A., Goosse, H., Kamenkovich, I., Knutti, R., Lohmann, G., Marsh, R., Mysak, L. A., Wang, Z., and Weaver, A. J.: Thermohaline circulation hysteresis: A model intercomparison, Geophys. Res. Lett., 32(23), L23605, doi:10.1029/2005GL023655, 2005. 227
Reeh, N., Mayer, C., Miller, H., Thomson, H. H., and Weidick, A.: Present and past climate control on fjord glaciations in Greenland: Implications for IRD-deposition in the sea, Geophys. Res. Lett., 26, 1039–1042, 1999. 231, 236
Ridley, J., Huybrechts, P., Gregory, J. M., and Lowe, J.: Elimination of the Greenland ice sheet in a high-CO_2 climate, J. Climate, 18(17), 3409–3427, 2005. 236
Rignot, E. and Kanagaratnam, P.: Changes in the Velocity Structure of the Greenland Ice Sheet, Science, 311, 986–990, doi: 10.1126/science.112138, 2006. 232
Solomon, S., Qin, D., Manning, M., Alley, R. B., Berntsen, T., Bindoff, N. L., Chen, Z., Chidthaisong, A., Gregory, J. M., Hegerl, G. C., Heimann, M., Hewitson, B., Hoskins, B. J., Joos, F., Jouzel, J., Kattsov, V., Lohmann, U., Matsuno, T., Molina, M., Nicholls, N., Overpeck, J., Raga, G., Ramaswamy, V., Ren, J., Rusticucci, M., Somerville, R., Stocker, T. F., Whetton, P., Wood, R. A., and Wratt, D.: Technical Summary. In: Climate Change 2007: The Physical Science Basis, Contribution of Working Group I to the Fourth Assessment Report of the Intergovernmental Panel on Climate Change (IPCC AR4), edited by: Solomon, S., Qin, D., Manning, M., Chen, Z., Marquis, M., Averyt, K. B., Tignor, M., and Miller , H. L., Cambridge University Press, Cambridge, United Kingdom and New York, NY, USA, 2007. 226
Swingedouw, D., Braconnot, P., and Marti, O.: Sensitivity of the Atlantic Meridional Overturning Circulation to the melting from northern glaciers in climate change experiments, Geophys. Res. Lett., 33, L07711, doi:10.1029/2006GL025765, 2006. 227
Uppala, S. M., Kallberg, P. W., Simmons, A. J., Andrae, U., da Costa Bechtold, V., Fiorino, M., Gibson, J. K., Haseler, J., Hernandez, A., Kelly, G. A., Li, X., Onogi, K., Saarinen, S., Sokka, N., Allan, R. P., Andersson, E., Arpe, K., Balmaseda, M. A., Beljaars, A. C. M., van de Berg,

L., Bidlot, J., Bormann, N., Caires, S., Chevallier, F., Dethof, A., Dragosavac, M., Fisher, M., Fuentes, M., Hagemann, S., Holm, E., Hoskins, B. ., Isaksen, L., Janssen, P. A. E. M., Jenne, R., McNally, A. P., Mahfouf, J.-F., Morcrette, J.-J., Rayner, N. A., Saunders, R. W., Simon, P., Sterl, A., Trenberth, K. E., Untch, A., Vasiljevic, D., Viterbo, P., and Woollen, J.: The ECMWF re-analysis, Q. J. Roy. Meteor. Soc., 131, 2961–3012, doi:10.1256/qj.04.176, 2005. 242

Vinther, B. M., Andersen, K. K., Jones, P. D., Briffa, K. R., and Cappelen, J.: Extending Greenland temperature records into the late eighteenth century, J. Geophys. Res., 111, D11105, doi:10.1029/2005JD006810, 2006. 230

Zwally, J. H., Abdalati, W., Herring, T., Larson, K., Saba, J., and Steffen, K.: Surface Melt-Induced Acceleration of Greenland Ice-Sheet Flow, Science, 297, 218–222, 2002. 232, 236

Table 1. Five climatological data sets used in this paper to estimate the GrIS SMB.

Abbreviation	Name	Period	Resolution	Web site	Reference
CRU	Climate Research Unit TS 2.1	1901–2002	0.5°	http://www.cru.uea.ac.uk	Mitchell and Jones (2005)
ECMWF	ECMWF (Re)-Analysis	1958–2006	1.125°	http://www.ecmwf.int	Uppala et al. (2005)
GHCN	Global Histo. Climato. Network 2	1900–2006	5°	http://lwf.ncdc.noaa.gov/	Peterson and Vose (1997)
NCEP	NCEP/NCAR Reanalysis 1	1948–2006	~2°	http://www.cdc.noaa.gov/cdc/data.ncep.reanalysis.html	Kalnay et al. (1996)
UDEL	Arctic Land-Surface TS 1.01	1930–2000	0.5°	http://climate.geog.udel.edu/~climate/html_pages/download.html#ac_temp_ts2	

Table 2. Correlation coefficient between the de-trended annual temperature (resp. precipitation) anomaly averaged over Region 1 (resp. Region 2) from the different data sets and simulated by the MAR model over the reference period (1970–1999). The correlation coefficient as well as the RMSE (in km^3) between the de-trended GrIS SMB modelled by MAR and the SMB estimated by temperature/precipitation de-trended anomaly time series are also shown. Finally, the last column lists the ratio of the parameters a and b computed by using de-trended normalised time series.

Name	ΔT corr.	ΔP corr.	ΔSMB	RMSE	a/b
CRU	0.79	0.84	0.81	64.6	−1.32
ECMWF	0.92	0.94	0.89	49.3	−1.57
GHCN	0.83	0.82	0.83	61.4	−0.87
NCEP	0.91	0.90	0.89	49.6	−1.73
UDEL	0.86	0.80	0.83	61.0	−1.76
MAR	1.0	1.0	0.97	28.7	−1.47

Table 3. The same as Table 2 but by using results simulated by Hanna08 in the left part of Eq. (1).

Name	ΔSMB	RMSE	a/b
CRU	0.86	52.3	−0.95
ECMWF	0.97	26.1	−1.17
GHCN	0.86	52.5	−0.63
NCEP	0.96	30.7	−1.34
UDEL	0.86	52.2	−1.25

Table 4. Twenty-four AOGCMs from the IPCC AR4 used in this paper. This data comes from the World Climate Research Programme's (WCRP's) Coupled Model Intercomparison Project phase 3 (CMIP3) multi-model dataset available at http://www-pcmdi.llnl.gov/.

Nodel ID	Sponsors, Country
BCCR-BCM2.0	Bjerknes Centre for Climate Research, Norway
CCSM3	National Center for Atmospheric Research, USA
CGCM3.1(T47/T63)	Canadian Centre for Climate Modelling and Analysis, Canada
CNRM-CM3	Météo-France/Centre National de Recherches Météorologiques, France
CSIRO-MK3.0/3.5	Commonwealth Scientific and Industrial Research Organisation Atmospheric Research, Australia
ECHAM5-MPI-OM	Max Planck Institute for Meteorology, Germany
ECHO-G	Meteorological Institute of the University of Bonn, Germany Meteorological Research Institute of the Korea Meteorological Administration Korea
FGOALS-g1.0	National Key Laboratory of Numerical Modeling for Atmospheric Sciences and Geophysical Fluid Dynamics /Institute of Atmospheric Physics, China
GFDL-CM2.0/2.1	US Department of Commerce/National Oceanic and Atmospheric Administration/Geophysical Fluid Dynamics Laboratory, USA
GrISS-AOM	National Aeronautics and Space Administration /Goddard Institute for Space Studies, USA
GrISS-EH/ER	National Aeronautics and Space Administration /Goddard Institute for Space Studies, USA
INM-CM3.0	Institute for Numerical Mathematics, Russia
IPSL-CM4	Institut Pierre Simon Laplace, France
MIROC3.2(hires)/(medres)	Center for Climate System Research, National Institute for Environmental Studies, and Frontier Research Center for Global Change, Japan
MRI-CGCM2.3.2	Meteorological Research Institute, Japan
PCM	National Center for Atmospheric Research, USA
UKMO-HadCM3/HadGEM1	Hadley Centre for Climate Prediction and Research/Met Office, UK

Table 5. Future projections for the 21st century from the ensemble mean of the AOGCMs simulations performed for the IPCC AR4. The two last lines use simulations made for the SRESA2 experiments against SRESA1B for the other ones.

Decade	ΔT (in K°)	ΔP (in mm)	ΔSMB (in km^3) for $a/b=-1$	ΔSMB (in km^3) for $a/b=-2$
2010–2019	0.62	9.32	−55±61	−83±65
2020–2029	0.8	16.18	−65±36	−102±44
2030–2039	1.13	41.99	−85±59	−140±64
2040–2049	1.37	48.34	−93±51	−165±57
2050–2059	1.63	37.14	−139±76	−214±75
2060–2069	1.79	26.70	−153±76	−234±80
2070–2079	2.09	50.28	−167±74	−268±87
2080–2089	2.22	76.04	−177±81	−284±90
2090–2099	2.33	40.95	−185±82	−298±96
2080–2089	2.49	71.62	−209±134	−328±157
2090–2099	2.77	86.34	−220±120	−355±148

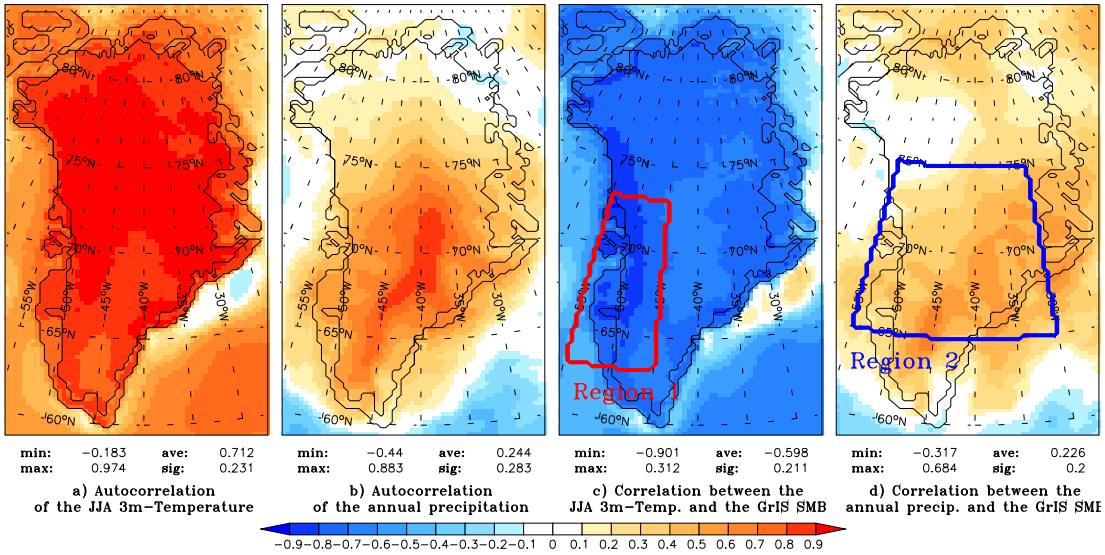

Fig. 1. Left: autocorrelation of the **(a)** JJA 3 m-temperature and **(b)** annual precipitation simulated by MAR over the period 1970–1999. The autocorrelation is defined as the correlation between time series of the average ice-sheet summer temperature and annual total ice-sheet precipitation with the respective temperature/precipitation values for each grid point. Right: the correlation between the time series of the MAR-simulated GrIS SMB and **(c)** JJA 3 m-temperature and **(d)** annual precipitation at each grid location. Minimum and maximum values are indicated as well as the ice sheet average and the standard deviation. Finally, this figure shows the regions quoted in the text. Region 1: 55° W≤longitude≤45° W and 63° N≤latitude≤73° N. Region 2: 55° W≤longitude≤30° W and 65° N≤latitude≤75° N.

TCD
2, 225–254, 2008

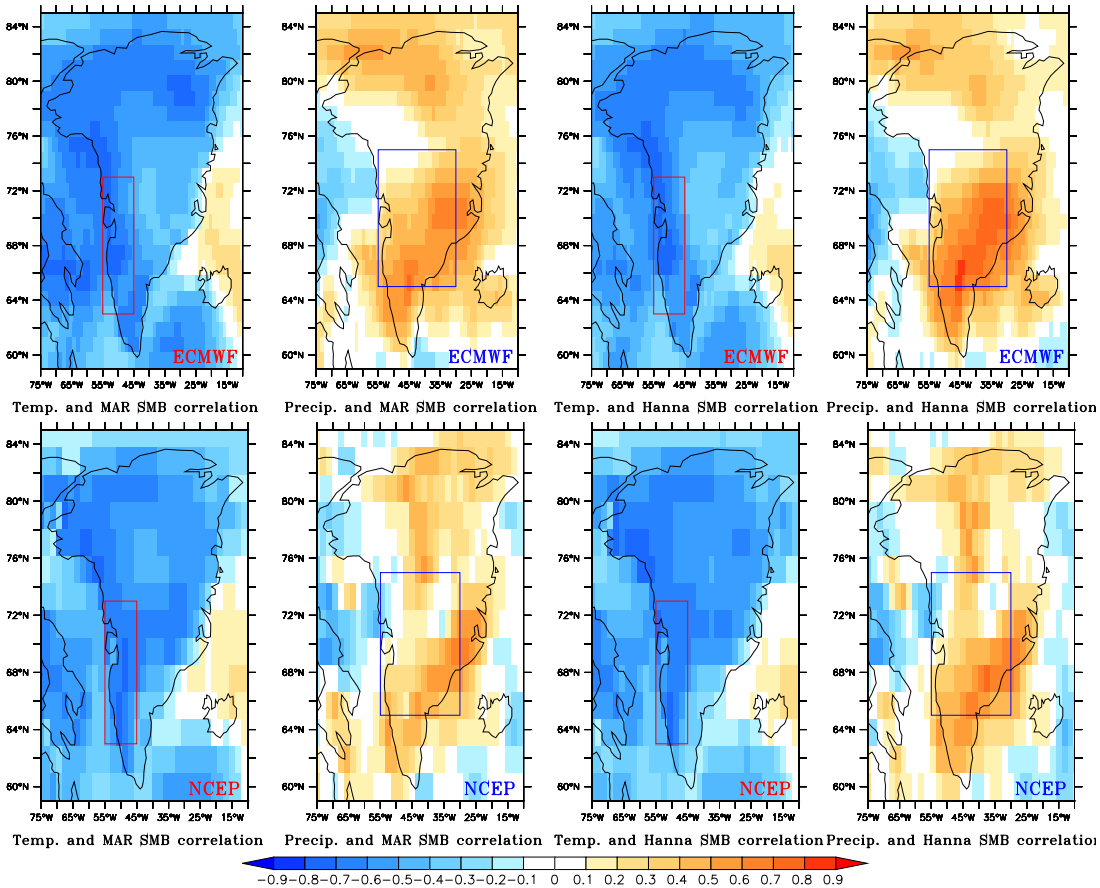

Fig. 2. Correlation between the time series of the MAR (resp. Hanna08) simulated GrIS SMB and the summer 3 m-temperature and annual precipitation from the ECMWF (resp. NCEP/NCAR) reanalysis at each grid location over 1970–1999.

TCD
2, 225–254, 2008

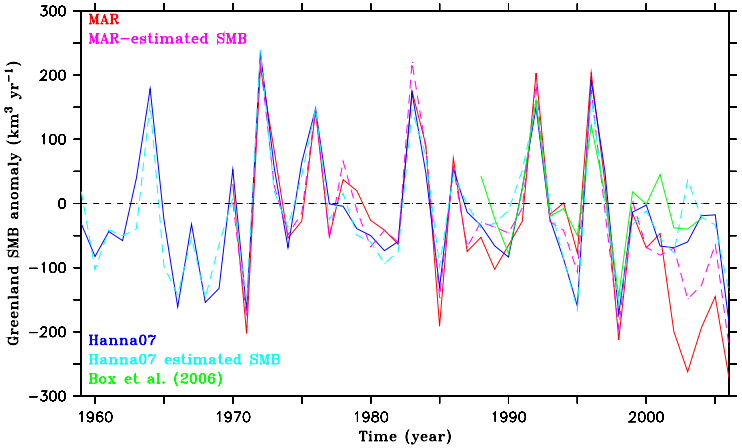

Fig. 3. The GrIS SMB anomaly simulated by the MAR model and estimated with Eq. (1) by using temperature/precipitation anomaly simulated by MAR, derived using a positive degree-day and runoff/retention model based on ECMWF reanalysis Hanna et al. (2008) and estimated by using temperature/precipitation anomaly from the ECMWF (re)analysis, and simulated by the Polar MM5 model Box et al. (2006). The reference period is 1970–1999 and the temperature and precipitation anomaly are taken from Region 1 and 2 described in Fig. 1.

TCD
2, 225–254, 2008

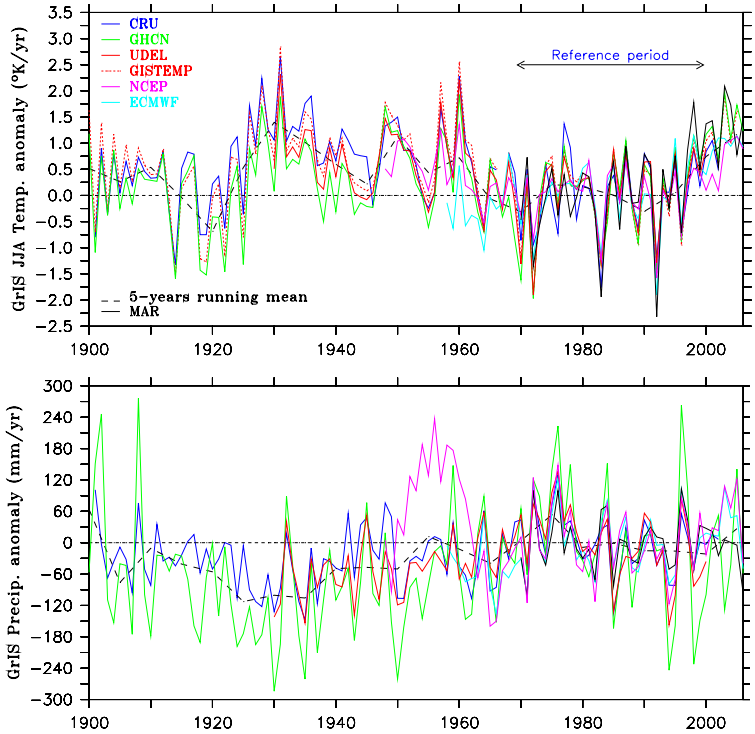

Fig. 4. Time series of the GrIS temperature (resp. precipitation) anomaly computed for Region 1 (resp. 2) from the different data sets listed in Table 1. In red dashed, the time series from GISTEMP (available at http://data.giss.nasa.gov/). Anomalies are with respect to 1970–1999. The 5-yr running mean of the averaged anomalies of the available data sets is shown in dashed black.

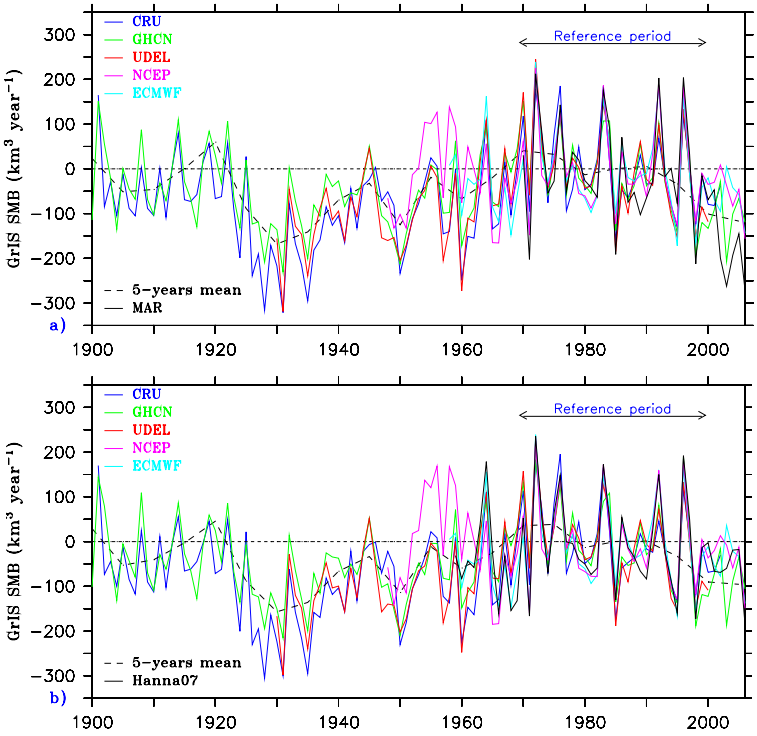

Fig. 5. (a) Time series of the estimated GrIS SMB anomaly using the SMB variability simulated by MAR (to determine the parameters *a* and *b* in Eq. (1)) and anomalies from the different data sets listed in Table 1 since 1900 until 2006. The reference period is 1970–1999 over which the GrIS SMB simulated by MAR and by Hanna08 is around 350 $km^3\,yr^{-1}$. The 5-yr running mean of the ensemble mean is shown in dashed black. **(b)** The same as (a) but using the Hanna08 results to determine the parameters *a* and *b* in Eq. (1).

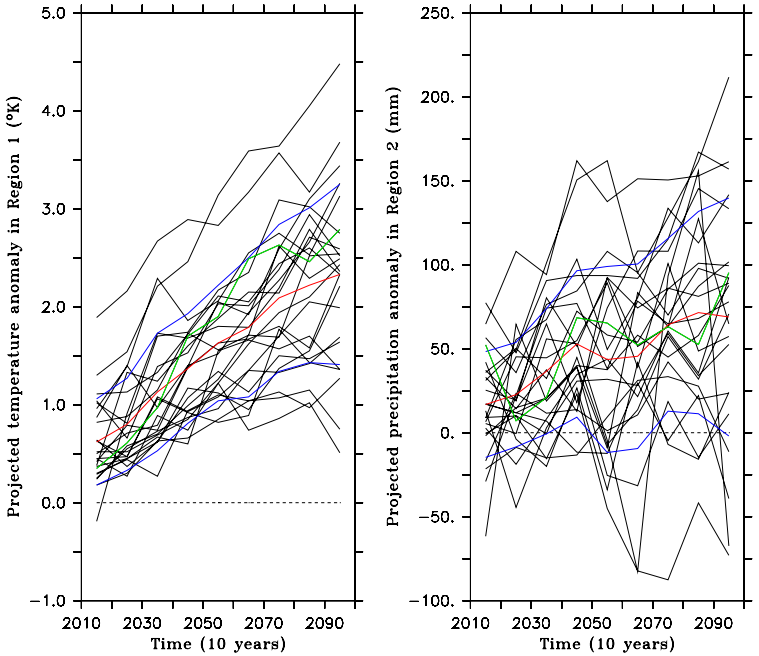

Fig. 6. Time series of temperature (resp. precipitation) anomalies projected by AOGCMs listed in Table 4. The anomalies are decadal means, computed on Region 1 and 2 described previously and refer to the period 1970–1999. The anomalies are based on model outputs from the "Climate of the Twentieth Century Experiment" (20C3M) and from the scenario SRES A1B. Finally, the ensemble mean (i.e. the anomalies averaged over all the available models), the standard deviation and the UKMO-HadCM3 time series are plotted in red, blue and green, respectively.

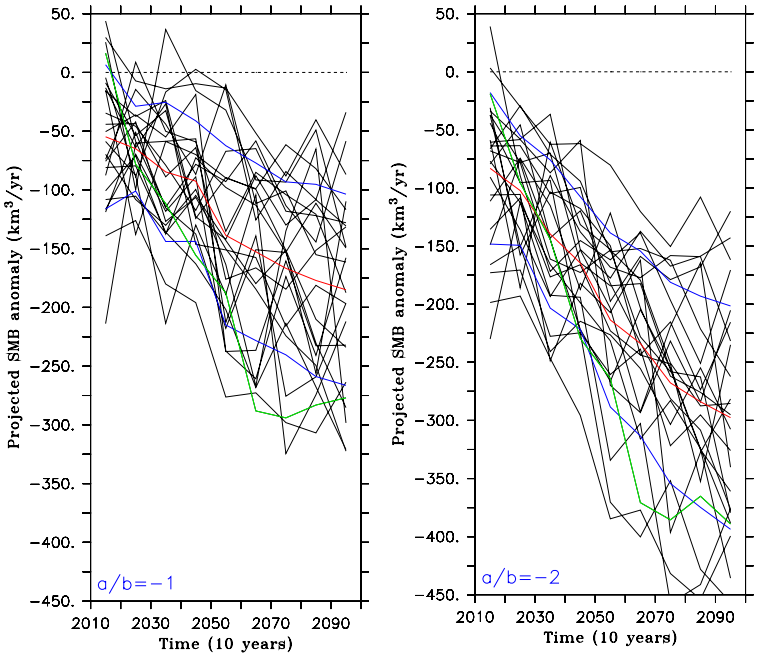

Fig. 7. Time series of SMB anomalies projected by AOGCMs listed in Table 4 for a/b=−1 and a/b=−2. The anomalies are decadal means and refer to 1970–1999. The anomalies are based on model outputs from the "Climate of the Twentieth Century Experiment" (20C3M) and from the scenario SRES A1B. Finally, the ensemble mean (i.e. the anomalies averaged over all the available models), the standard deviation and the UKMO-HadCM3 time series are plotted in red, blue and green, respectively.

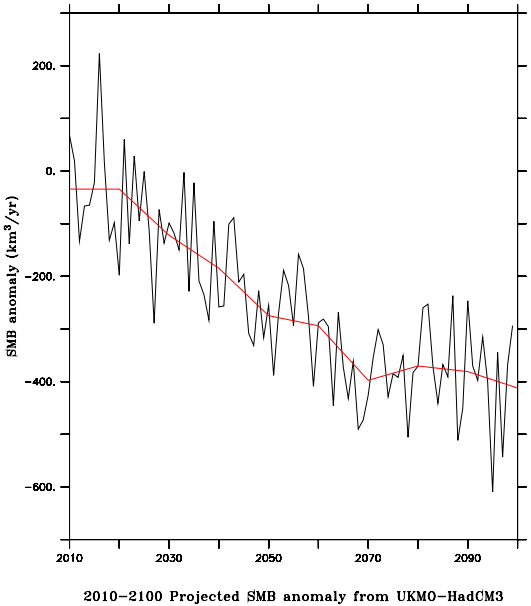

Fig. 8. The 2010–2100 projected SMB anomaly using temperature/precipitation anomaly simulated by UKMO-HadCM3 for $k=-2$. The temperature/precipitation projections from UKMO-HadCM3 are near the ensemble mean and its SMB anomaly projections are at the negative end compared with other models. The 10-yr running mean is shown in red.

TCD
2, 225–254, 2008